

## Pressure-temperature-reaction history of metapelitic rocks from the Maryland Piedmont on the basis of correlated garnet zoning and plagioclase-inclusion composition

HELEN M. LANG

Department of Geology and Geography, West Virginia University, P.O. Box 6300, Morgantown, West Virginia 26506-6300, U.S.A.

### ABSTRACT

Regional structural interpretation, thermobarometry, and Gibbs-method calculations were combined to determine an approximate  $P$ - $T$  path for kyanite-grade metapelitic rocks of the Baltimore Gneiss terrane. Garnet growth along the estimated  $P$ - $T$  path was modeled using the computer program DiffGibbs. Models were evaluated by comparing calculated profiles of garnet components with measured profiles of a large garnet rich in plagioclase inclusions in a kyanite-bearing sample from the area. Modifications in the  $P$ - $T$  path constrained by changes in garnet components along critical portions of the profile resulted in a very satisfactory match between measured and model-garnet profiles. In the most successful model, garnet growth began at 550 °C and 6500 bars in the assemblage chlorite + biotite + garnet + muscovite + plagioclase + quartz with increasing temperature and with decreasing and then constant pressure. At 570 °C and 5724 bars, staurolite was added to the assemblage and some garnet was consumed. In the model, garnet growth resumed after chlorite was consumed along a path having a substantial increase in pressure. The region near the rim with low measured grossular content was reproduced by cessation of garnet growth as temperature increased at constant pressure to a maximum of 615 °C at 6474 bars. After kyanite was added to the assemblage, grossular increased to the constant rim value only if temperature decreased and pressure increased. Cooling and decompression affected garnet zoning only very near the rim. Measured compositions of the rims of plagioclase inclusions in the garnet are consistent with plagioclase compositions predicted by the model.

This study demonstrates that complex garnet zoning can be modeled successfully, even when the reaction history includes episodes of garnet consumption, over a path that is consistent with geologic evidence. Details of garnet zoning provide surprisingly tight constraints on the  $P$ - $T$  path.

### INTRODUCTION

In the last decade, it has been increasingly appreciated that metamorphic rocks reached their peak conditions along a variety of pressure-temperature-time paths depending on their thermal and tectonic history (e.g., Thompson and England 1984; England and Thompson 1984; Brown 1993). Zoned metamorphic garnet provides a record of the history of pressure, temperature, and reaction changes in a metamorphic rock if it can be correctly interpreted (Tracy et al. 1976; Spear and Selverstone 1983; Spear et al. 1984; Spear and Florence 1992; Florence and Spear 1993). If the garnet contains inclusions, additional evidence about the early history of the rock may be available (Thompson et al. 1977; St-Onge 1987). Plagioclase inclusions are particularly informative because garnet and plagioclase are commonly the only calcic phases in pelitic rocks and plagioclase is very refractory to Ca exchange (Spear et al. 1990; Kohn et al. 1992).

Most of the techniques that have been proposed for

interpreting garnet zoning begin with an estimate of the “peak metamorphic conditions” at the garnet rim (Spear and Selverstone 1983; Spear et al. 1984; St-Onge 1987). They then step back along the  $P$ - $T$  path using compositions of garnet and inclusions closer to the center of the garnet. These techniques do not, in general, incorporate the constraints of mass balance or the effects of diffusion.

A computer algorithm for “forward modeling” of garnet growth (that is, modeling of garnet growth and composition from its initiation at the garnet isograd throughout the pressure-temperature-reaction history of the rock) was developed by Spear and Florence (Spear 1988; Florence and Spear 1991, 1993; Spear and Florence 1992). This technique, which is incorporated into the computer program DiffGibbs (Spear 1990), monitors mass balance as garnet is fractionally crystallized and includes the effects of diffusion. It allows one to follow the crystallization of a particular starting assemblage along an inferred  $P$ - $T$  path and predicts the garnet zoning and changes in assemblage that would result. This technique

provides a sensitive test of many inferences about the evolution of a metamorphic rock.

Metamorphosed pelitic rocks from the kyanite zone of the Baltimore Gneiss terrane in eastern Maryland (Lang 1990, 1991) contain garnet grains (commonly 6–7 mm in diameter) that are zoned and that contain abundant plagioclase inclusions. These rocks are ideally suited for demonstrating the usefulness of garnet-growth and diffusion modeling using the program DiffGibbs (Spear 1990) because garnet zoning and plagioclase-inclusion composition can be correlated. The DiffGibbs program plots a garnet compositional profile after each increment of growth and diffusion and monitors changes in mode and composition of other minerals. Inferences about the pressure-temperature-reaction history of these rocks were tested and refined by examining the correspondence of measured and calculated garnet profiles, modes, and plagioclase composition.

### GEOLOGIC SETTING

The northeast-southwest belt of metamorphic rocks northwest of Baltimore, Maryland, that includes exposures of the Baltimore Gneiss is commonly designated the Baltimore Gneiss terrane (Fig. 1a). The Grenville-age Baltimore Gneiss and overlying sediments were thrust northwestward into a nappe structure and metamorphosed during the Ordovician Taconic Orogeny (Fig. 1b; Crowley et al. 1976; Fisher et al. 1979; Muller and Chapin 1984; Sinha 1988; Fisher 1989). Metasedimentary units exposed in the area surrounding the Baltimore Gneiss include quartzites and pelites of the Setters Formation, the Cockeysville Marble, and pelitic schists of the Loch Raven Schist (Fig. 1a). Metapelitic rocks in the area reached maximum metamorphic grade in the staurolite + kyanite to kyanite + sillimanite zones (Lang 1990, 1991). The freshest samples of pelitic schist come from a one-half mile long exposure of the garnet schist member of the Setters Formation (Crowley et al. 1976) behind the Hunt Valley Mall approximately 20 km north of Baltimore.

### Deformation

Three stages of deformation that were approximately synchronous with metamorphism affected pelitic schists in the Baltimore Gneiss terrane (Hall 1988). These stages, which correspond to the  $F_{2a}$ ,  $F_{2b}$ , and  $F_{2c}$  generations of folding recognized by Muller and Chapin (1984) in the Baltimore Gneiss, were caused by collision of the Baltimore Mafic Complex island arc terrane with the Baltimore Gneiss terrane during the Ordovician Taconic Orogeny (Sinha 1988).  $F_{2a}$  was attributed to nappe formation by Muller and Chapin (1984).  $F_{2b}$ , which was primarily a flattening deformation, refolded the nappe(s) (Fig. 1b) and produced the dominant schistosity and the map pattern of gneiss-cored anticlines (Fig. 1a).  $F_{2c}$  produced mesoscopic folds with horizontal axial planes and crenulated the  $F_{2b}$  foliation.

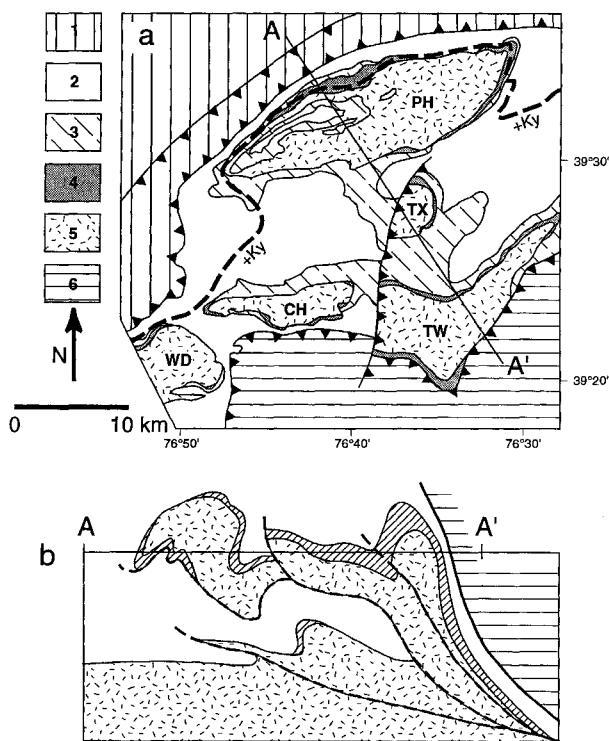


**FIGURE 1.** (a) Generalized geologic map of the eastern Maryland Piedmont (after Fisher 1989; Muller et al. 1989; Crowley et al. 1976). 1 = Low- to medium-grade metasediments of the western Piedmont; 2 = Loch Raven Formation, mainly pelitic schist; 3 = Cockeysville Marble; 4 = Setters Formation, quartzite and pelitic schist; 5 = Baltimore Gneiss, felsic basement gneiss; 6 = Baltimore Mafic Complex, island arc complex that collided with the Baltimore Gneiss terrane (units 2–5) during the Taconic Orogeny (at approximately 470 Ma). Anticlines in which the Baltimore Gneiss is exposed are labeled PH (Phoenix), TX (Texas), TW (Towson), CH (Chattolane), and WD (Woodstock). The line labeled A-A' shows the approximate location of the schematic cross section shown in b. (b) Schematic cross section A-A' through the Baltimore area after Fisher (1989). The random dash pattern represents the Baltimore Gneiss; the diagonal line pattern represents the Cockeysville and Setters Formations combined; the unpatterned area is the Loch Raven Formation, and the horizontal line pattern represents the Baltimore Mafic Complex. Bold dashed lines indicate thrust faults inferred by Fisher on the basis of the structural style of similar units in the Philadelphia area.

### Metamorphism

There is evidence for only one protracted metamorphic episode that spanned  $D_2$  deformation. No pseudomorphs after staurolite or aluminosilicate minerals or relict minerals that might indicate an earlier episode of metamorphism were observed. Most samples to the southeast of the generalized kyanite isograd shown in Figure 1a contain kyanite; however, staurolite (without kyanite), staurolite + kyanite, kyanite, and kyanite + sillimanite assemblages are distributed in an unsystematic way within this zone (Lang 1990). Variation in metamorphic assem-

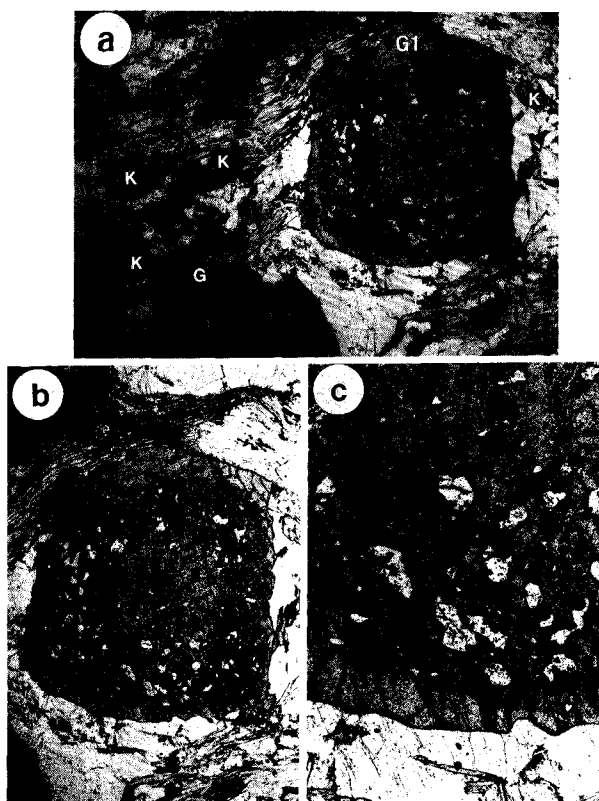


**FIGURE 2.** (a) Low-magnification photomicrograph of sample HV104, showing the relationship of the model garnet (G1) to the fabric and other phases in the sample. Staurolite (S with arrows, in lower right), kyanite (K), and another garnet (G) are labeled. The long dimension of the photomicrograph is approximately 13 mm. (b) Photomicrograph of the largest garnet in sample HV104, which is the basis for the modeling. Note the core, the intermediate plagioclase inclusion-rich region, and the inclusion-free rim of the garnet. The long dimension of the photomicrograph is approximately 10 mm. (c) A higher magnification photomicrograph of the lower, middle part of the garnet shown in **b**. The photograph shows the intermediate region of the garnet, which contains abundant plagioclase inclusions (bright, low-relief areas), and a portion of the inclusion-free rim. Note the faceted, negative garnet crystal shape of some of the inclusions and the dusty appearance produced by abundant small inclusions. The long dimension of the photomicrograph is approximately 3 mm. Maps of the anorthite content in plagioclase and the grossular content in garnet of the central portion of this area are shown in Figure 5.

blage was shown to be a function of variation in both fluid composition and bulk composition across the one-half mile long Hunt Valley Mall exposure within this zone (Lang 1991).

Two mineral assemblages that are common in samples from the kyanite zone were referred to by Lang (1991) as the staurolite (St) assemblage and the staurolite + kyanite (St + Ky) assemblage. The staurolite assemblage contains abundant, commonly porphyroblastic staurolite, garnet, biotite, quartz, muscovite, plagioclase (which

commonly occurs as ovoid porphyroblasts), ilmenite, and magnetite. The staurolite + kyanite assemblage (Fig. 2a) contains abundant kyanite, only minor, fine-grained staurolite, garnet, biotite, quartz, muscovite, plagioclase, ilmenite, rutile, and pyrrhotite. No graphite was observed in either assemblage. Some St and some St + Ky assemblages contain small amounts of chlorite, most of which is interpreted to be retrograde.

Because this paper focuses on garnet growth and zoning, textures of garnet grains are described in detail. In a given hand specimen, garnet grains are fairly uniform in size and exhibit similar textures. In some samples, commonly those that contain kyanite, garnet grains are large (on the order of 6 mm in diameter) with poikiloblastic cores that are dusty with fine inclusions and that contain abundant, relatively large plagioclase inclusions (Fig. 2). These grains have inclusion-free idioblastic to hypidioblastic rims. Garnet growth in these samples began after  $F_{2a}$  and continued through  $F_{2b}$  (Hall 1988). The inclusion-free rims may have continued to grow during or after  $F_{2c}$ . Some of the staurolite-bearing samples that lack kyanite also contain large poikiloblastic garnet grains, but some contain small idioblastic, nearly inclusion-free grains that appear to be almost entirely postkinematic (Hall 1988). Staurolite grew during  $F_{2b}$ , and kyanite grew mainly after  $F_{2b}$  but was folded by  $F_{2c}$ . Sillimanite is abundant in only a few samples. Many of the staurolite + kyanite and kyanite samples, however, contain small amounts of very fine prismatic sillimanite. In every case, sillimanite appears to have grown late in the metamorphic episode. It is believed to have formed during decompression at or near the maximum temperature (Lang 1990).

#### Tectonothermal constraints

Major deformation and metamorphism in the Maryland Piedmont apparently occurred during the Ordovician Taconic orogeny before the intrusion of the Ellicott City granodiorite at 458 Ma (Sinha 1988). The Ellicott City pluton is an epidote-bearing pluton, which must have intruded at relatively great depth. Limited data indicate that late Paleozoic deformation and metamorphism in Maryland were restricted to shear zones (Sutter 1994, personal communication). Cooling dates for these rocks may have been on the order of 450 Ma, and the duration of the heating event may have been about 500–450 Ma. Geochronologic studies currently in progress (Sutter 1994, personal communication) may provide additional indications of the tectonothermal history of the area.

#### ANALYTICAL METHODS

Mineral compositions were determined by analyzing carbon-coated, polished thin sections on the ARL-SEM-Q microprobe at Virginia Polytechnic Institute and State University. Operating conditions were 15 kV accelerating potential and 20 nA beam current. A focused beam  $\sim 1 \mu\text{m}$  in diameter was used for garnet and other minerals in which volatile loss was not likely to be a problem. A  $4 \times 4 \mu\text{m}$  raster was used for micas and plagioclase to

TABLE 1. Mean compositions of matrix phases in HV104

	Muscovite	Biotite	Garnet rim	Staurolite	Plagioclase
SiO <sub>2</sub>	44.83	35.69	37.73	27.50	61.15
TiO <sub>2</sub>	0.66	1.62	0.10	0.62	0.03
Al <sub>2</sub> O <sub>3</sub>	34.95	19.82	21.63	53.80	24.28
FeO	1.18	17.86	35.50	12.57	0.12
MnO	0.01	0.06	0.72	0.04	0.01
MgO	0.91	11.74	3.99	1.87	0.18
CaO	0.04	0.09	1.78	0.03	4.82
Na <sub>2</sub> O	1.20	0.23	0.01	0.07	8.72
K <sub>2</sub> O	8.89	8.52	0.03	0.02	0.06
Other	F = 0.06	F = 0.39		ZnO = 1.46	
Total	92.65	95.61	101.51	97.96	99.37
Cations per X anh. O atoms	22	22	12	46	8
Si	6.098	5.329	2.978	7.640	2.729
Ti	0.067	0.182	0.006	0.129	0.001
Al	5.606	3.489	2.012	17.620	1.277
Fe	0.135	2.230	2.343	2.920	0.005
Mn	0.001	0.007	0.048	0.009	0.001
Mg	0.184	2.613	0.469	0.774	0.012
Ca	0.006	0.014	0.151	0.009	0.231
Na	0.316	0.065	0.002	0.037	0.755
K	1.543	1.624	0.003	0.008	0.003
Other	F = 0.024	F = 0.184		Zn = 0.299	
Total	13.956	15.553	8.013	29.444	5.011

prevent loss of volatile elements. Standard nine-element analyses were performed for most minerals. Eighteen-element analyses (Solberg and Spear 1982) were performed on a few grains of staurolite, biotite, and muscovite in each sample to determine Zn and F and to detect other minor elements. Well-characterized natural standards were used for most elements; synthetic oxide or glass standards were used for a few minor elements. Data reduction was performed according to the procedure of Bence and Albee (1968) with the alpha factors of Albee and Ray (1970). All Fe was reported as FeO. Mean compositions (at least six spots per mineral) of matrix phases in sample HV104 are given in Table 1.

Qualitative images of garnet composition for some samples from the Baltimore Gneiss terrane were prepared on the microprobe at Virginia Polytechnic Institute and State University. Semiquantitative molar maps of garnet composition for a few samples were prepared from data collected on the automated JEOL 733 electron microprobe at Rensselaer Polytechnic Institute (R.P.I.) with the use of an X-ray mapping technique developed by Wark and Spear (unpublished manuscript). The microprobe stage was programmed to step across a rectangular grid under a fixed beam with step sizes and count times adjusted to get reasonable counting statistics in overnight experiments. A beam current of approximately 100–140 nA was used to excite the sample. Counts were continuously collected on five fixed, wavelength-dispersive spectrometers, which were set for Na, Ca, Mg, Mn, and Fe, and the energy-dispersive detector, which was set for Al, Si, K, Ti, and background. The wavelength-dispersive spectrometers were calibrated against well-characterized mineral standards.

Garnet molar maps or images were made from the uncorrected (for background and matrix effects) weight percents with the use of the Xraymap11 program (Spear,

unpublished manuscript). Weight percents of CaO, MgO, MnO, and FeO are converted to moles by dividing by their respective molecular weights, and the mole fractions of garnet components are calculated and stored in corresponding pixels of four separate images. Values of moles of Fe/(Fe + Mg) are stored in the pixels of a fifth image. A molar image of the anorthite content of plagioclase is created in a similar fashion from the original image.

Detailed traverses of the garnet from HV104 that was the subject of DiffGibbs modeling were performed at R.P.I. and on the Duke University of North Carolina microprobe (D.L. Whitney, personal communication). Standard quantitative spot-analysis techniques were used at 100–200 spots along a programmed line traverse. Multiple quantitative analyses across a few plagioclase inclusions in the HV104 garnet were also performed on the Duke University of North Carolina microprobe (D.L. Whitney, personal communication).

## GARNET ZONING

### General features

X-ray maps and microprobe traverses of several of the large, inclusion-rich garnets that are common in samples inside the kyanite isograd in Figure 1a (both staurolite- and staurolite + kyanite-bearing samples) show that they have many features in common. In most of these garnets, grossular and spessartine contents decrease from core to rim, and pyrope and almandine contents increase from core to rim. Garnet zoning is concentric and is not related to inclusions, fractures, or other textural features. Fe/(Fe + Mg) is fairly uniform in the cores of these garnets and decreases toward the rims. There are complexities in many profiles, and all components are likely to show a sharp reversal in trend at the rim of the garnet. Many of these garnets have a patchy, irregular region in their cores

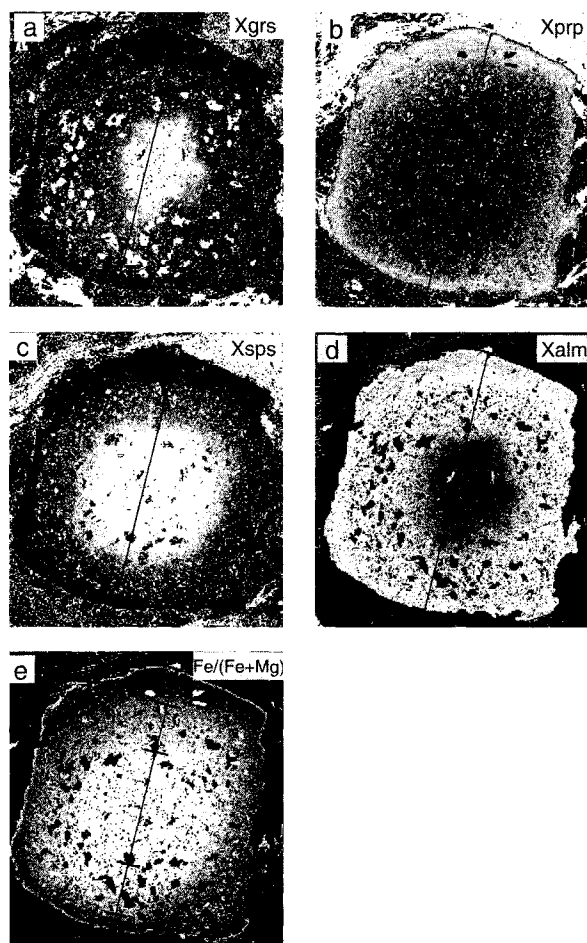


**FIGURE 3.** Gray scale maps of the mole fraction of components of the garnet shown in Figure 2b: (a) grossular, (b) pyrope, (c) spessartine, (d) almandine, and (e) Fe/(Fe + Mg). Bright areas have high concentration of a component, dark areas have low concentration. The gray scale on each map was adjusted separately to show the variation in concentration of that component. All images represent an area 6.5 mm wide by 6.9 mm high. The dark lines across the maps show the location of the profile along which the analyses shown in Figure 4 were taken. Line segments perpendicular to the line of the profile in e separate the garnet into core, intermediate shell, and rim regions that are referred to in the text.

that has relatively high grossular content. Spessartine exhibits a smoother, more symmetric, bell-shaped trend (probably owing to faster diffusion), and the highest spessartine content does not necessarily coincide with the highest grossular content. Almandine and pyrope maps and profiles show intermediate character. Another feature that is common to most of these garnets is a ring of relatively low grossular content, which is particularly apparent on the X-ray maps, as much as 20% of the radius inside the rim.

The polished thin section of sample HV104 contains several 5–7 mm diameter garnets that have abundant pla-

gioclase inclusions. The two garnets that were examined in detail exhibit the features that have been described above as typical of kyanite-zone garnet in the area. The largest garnet in the polished section from this sample was mapped and analyzed in great detail. This garnet was used as the basis for DiffGibbs modeling and the discussion that follows because it exhibits the features common to large, inclusion-rich garnet from the kyanite zone, it is likely to be a nearly central section, and it contains many plagioclase inclusions distributed throughout its volume. This garnet is also large enough that the interior has not been strongly affected by diffusion (Spear 1991).

#### Description of sample HV104

HV104 is a fairly typical example of the staurolite + kyanite assemblage from the Hunt Valley Mall exposure (Lang 1991). It contains the mineral assemblage kyanite + staurolite + garnet + biotite + muscovite + quartz + plagioclase + ilmenite + rutile + pyrrhotite. All these minerals coexist in apparent textural equilibrium. The sample is foliated, and mica-rich bands alternate with quartz-rich bands. The major foliation has been weakly folded by subsequent deformation. Muscovite defines the foliation, and biotite occurs both in the foliation and with more variable orientation elsewhere. Garnet occurs as large (commonly 5–7 mm) poikiloblastic porphyroblasts in the quartz-rich bands. Staurolite, which is relatively high in ZnO (1.4 wt%, Table 1), occurs as small xenoblastic, poikiloblastic crystals. Several grains of staurolite are associated with coarse-grained, randomly oriented muscovite crystals, although definitive replacement textures are absent. Kyanite, which contains relatively few ilmenite and biotite inclusions, is hypidioblastic and is larger and more abundant than staurolite. Kyanite occurs most commonly in the micaceous domains, and most crystals are elongated parallel to the foliation. Some kyanite crystals are bent. Minor clusters of late, fine-grained kyanite and sillimanite occur at garnet margins or plagioclase grain boundaries (Lang 1990). Plagioclase is abundant in the quartz-rich layers and occurs both as fine grains and as coarsely recrystallized grains. Matrix plagioclase is twinned and normally zoned. Although some quartz is fine grained (0.2–0.5 mm), much of the quartz is coarsely recrystallized, contains trails of fluid inclusions approximately perpendicular to the dominant foliation, and exhibits undulatory extinction and kink banding. Ilmenite is abundant, both in the matrix and as inclusions in garnet, pyrrhotite is present, and minor rutile occurs in association with matrix ilmenite (Lang 1990). Tourmaline is a relatively abundant accessory mineral; zircon and apatite are also present.

#### HV104 garnet

There are three petrographically definable regions in the garnet of HV104: an inner core, an intermediate shell, and the rim (Figs. 2b and 3e). Small, equant to slightly elongated, clear, low-relief, low-birefringence inclusions are fairly abundant in the core. These inclusions are prob-

ably mostly quartz. A few, slightly larger plagioclase inclusions occur in this core region. Ilmenite inclusions ( $0.1 \times 0.3$  mm) are common in the core and intermediate shell and less common in the rim. A few fractures cross this core region of the garnet.

The small quartz(?) inclusions are even more abundant in the intermediate shell, which also contains very small, unidentifiable inclusions that give it a "dusty" appearance (Figs. 2b and 2c). In addition, larger (0.2–0.3 mm diameter) plagioclase inclusions are abundant in this intermediate region. The plagioclase inclusions are equant with a hint of the faceted, negative garnet-crystal shape described by Whitney (1991). The plagioclase inclusions, in turn, commonly contain small, round, quartz inclusions. Zoning in the plagioclase inclusions is displayed petrographically by concentrically progressive extinction. The plagioclase inclusions are not commonly twinned, although twinning is prominent in matrix plagioclase. The chemical composition, zoning, and origin of the plagioclase inclusions are discussed further in a later section. Fractures are abundant in the inclusion-rich intermediate shell of the garnet. Rare biotite, chlorite, and muscovite inclusions occur out to the edge of the intermediate shell.

The garnet rim is nearly free of inclusions, except for a few grains of ilmenite and some large quartz grains that are continuous with the matrix. Relatively few fractures extend across the inclusion-free rim.

#### Molar maps of garnet components in the HV104 garnet

Grayscale molar maps of the four garnet components (grossular, pyrope, spessartine, and almandine) and  $\text{Fe}/(\text{Fe} + \text{Mg})$  of the largest garnet in HV104 are shown in Figure 3. Corresponding color images are available at the *American Mineralogist* World Wide Web site.<sup>1</sup> Grossular content in the garnet in Figure 3 ranges from 10 mol% in the core to 4 mol% near the rim (Fig. 4). In the core of the garnet there is an irregular lobate region with uniformly high grossular content. Because of its irregular, lobate shape, this region appears to be a remnant of a partially consumed garnet. The almandine image mirrors the grossular image with a similar irregular core with low almandine content (Fig. 3d). The spessartine, pyrope, and  $\text{Fe}/(\text{Fe} + \text{Mg})$  images display larger, more nearly spherical, core regions with high spessartine, low pyrope, and high  $\text{Fe}/(\text{Fe} + \text{Mg})$ , respectively. The difference in patterns is due in part to different sensitivities of the garnet components to variations in pressure and temperature (see modeling section) and in part to the more rapid diffusion of spessartine component.

#### Compositional profiles of HV104 garnet

Semiquantitative profiles of garnet composition can be taken directly from the molar garnet images with the use of the "profile" option of the NIH program IMAGE (version 1.49). Because fully quantitative profiles were deemed to be necessary for comparison with the model-

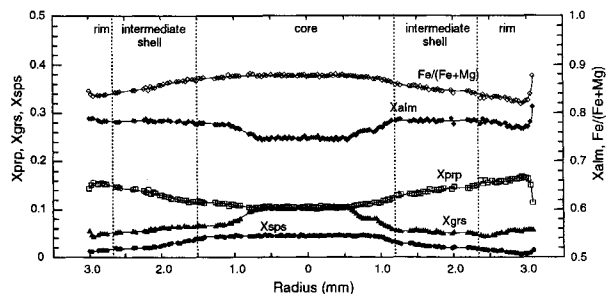


FIGURE 4. Profiles of mole-fraction almandine, pyrope, grossular, and spessartine components and  $\text{Fe}/(\text{Fe} + \text{Mg})$  across the garnet shown in Figures 2 and 3. The line of the profile is shown in Figure 3. The profiles from left to right go from bottom to top of the image. Profiles were assembled from closely spaced quantitative spot analyses along a traverse of the garnet. Symbols along the profiles represent individual spot analyses. The curves were fit by eye to the analyses. Dotted vertical lines separate the profile into core, intermediate shell, and rim regions, which are also indicated in Figure 3.

ing of garnet growth, a traverse of closely spaced, quantitative spot analyses was taken along the line shown in the garnet images in Figure 3. Note that the line of the profile crosses all the zones apparent in the images. Profiles of garnet composition in terms of mole fraction are shown in Figure 4. A few general features of the profiles are noteworthy. Some of these features are also apparent in the images in Figure 3. In general, grossular and spessartine components decrease from core to rim, and almandine and pyrope increase from core to rim.  $\text{Fe}/(\text{Fe} + \text{Mg})$  decreases very gradually out to one-half of the radius of the garnet and decreases more abruptly through the intermediate zone until very near the rim. Each of the garnet components has a relatively constant concentration in the core of the garnet, i.e., the profiles are relatively flat in the core region. Note particularly that the spessartine content is nearly constant to 1.0 mm from the center. Pyrope is constant to nearly the same position and begins to climb as spessartine decreases. Grossular content is nearly constant in the inner core, but it begins to decrease at about 0.7 mm (after a small but distinct upswing) before pyrope and spessartine begin to change. A step is apparent between 0.7 and 0.9 mm on the right side of the grossular profile. The outer step in the grossular profile coincides with the shoulders on the pyrope and spessartine profiles. The distribution of almandine component mirrors that of grossular component to a great extent. This is particularly apparent in the core regions of the grossular and almandine images (Fig. 3). Profiles for all components are nearly flat in the intermediate region of the garnet, with slight complexities such as the distinct near-rim low in the grossular profile (note the dark ring well inside the rim in Fig. 3a). There is a reversal in the general trend for each component at the rim of the garnet.

#### Plagioclase inclusions

The relatively large inclusions that appear as bright spots in the grossular image (Fig. 3a) and as dark spots

<sup>1</sup> The current URL is <http://ammin.gg.utk.edu>.

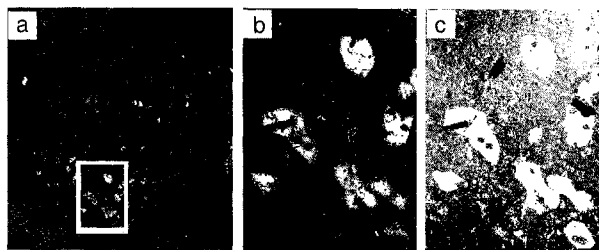


**FIGURE 5.** Molar X-ray maps of anorthite content of plagioclase inclusions and grossular in adjacent garnet. (a) Map of anorthite content of plagioclase for the entire garnet shown in Figure 2 (at the same scale as the garnet images of Fig. 3). Note the brighter, anorthite-rich plagioclase inclusions in the core, the intermediate brightness of plagioclase inclusions in the inclusion-rich intermediate shell, and the lower anorthite plagioclase outside the garnet. The bright spot in the upper left below the letter "a" is apatite. The white rectangle shows the area that is enlarged in **b** and **c**. (b) A more detailed map of the mole fraction of anorthite in plagioclase in a portion of the HV104 garnet. The center of the garnet is toward the upper right, and the image covers an area 1.3 mm wide and 1.8 mm high. All the plagioclase inclusions are normally zoned with higher anorthite in their cores and lower anorthite in the rims. Both the core and rim of the uppermost plagioclase inclusion are brighter, indicating higher anorthite content. (c) A detailed map of  $X_{\text{grossular}}$  for the same portion of the garnet shown in **b**. Grossular zoning in the garnet progresses from high values (bright) in the upper right corner, which is near the core, to low values at the bottom of the map, which is near the rim. There is no independent zoning in grossular around individual plagioclase inclusions (bright areas). Elongated inclusions that appear black are ilmenite; small, oval, speckled inclusions inside plagioclase inclusions are quartz.

on the compositional maps for the other garnet components (Figs. 3b–3e) are plagioclase. The plagioclase inclusions (Fig. 2c) have a hint of the faceted, negative garnet crystal shape noted by Whitney (1991) for plagioclase inclusions that she interpreted as having grown after entrapment in garnet. Plagioclase inclusions in the HV104 garnet and other garnets in kyanite-bearing rocks from the study area are interpreted as inclusions trapped during garnet growth for several reasons. They contrast with the plagioclase inclusions described by Whitney in several important ways. Details of zoning in the plagioclase inclusions and adjacent garnet appear on the molar maps shown in Figure 5 (corresponding color maps are available at the *American Mineralogist* web site). The X-ray map of mole-fraction anorthite for the whole garnet (Fig. 5a) shows that the anorthite content of plagioclase inclusions decreases systematically from the core to the rim of the garnet. This trend in plagioclase-inclusion composition is confirmed by approximate compositions of rims and cores of plagioclase inclusions taken directly from the image (NIH Image 1.49). Because plagioclase compositions taken from the image are not quantitative and show considerable scatter, a few plagioclase inclusions were quantitatively analyzed (D.L. Whitney, personal communication). Both core and rim compositions

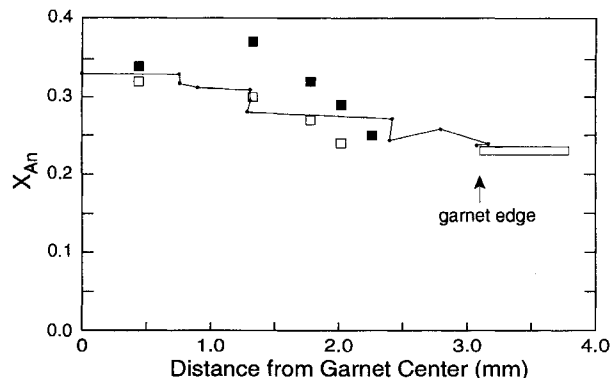


**FIGURE 6.** Graph of the composition of plagioclase inclusions vs. distance from the center of the garnet. The compositions shown are quantitative spot analyses of cores and rims of individual plagioclase inclusions. Cores of plagioclase inclusions are represented by solid squares, and rims are represented by open squares. The open bar beyond the garnet edge represents the average of spot analyses of matrix plagioclase rims. The line connecting small dots shows the composition of plagioclase calculated by the DiffGibbs model as a function of model-garnet radius.

of these plagioclase inclusions (Fig. 6) show a systematic decrease in anorthite content with distance from the garnet center.

More detailed images of a portion of the garnet and its plagioclase inclusions (Figs. 5b and 5c) show the nature of zoning in and adjacent to individual inclusions. The images show that these inclusions, in contrast to those described by Whitney (1991), are normally zoned (Fig. 5b). Normal zoning of the plagioclase inclusions was confirmed by a detailed microprobe traverse of one inclusion (the uppermost in Figs. 5b and 5c), in which anorthite content ranges from 0.37 in the core to 0.30 at the rim. There is no zoning of grossular (or any other garnet component) immediately adjacent to any plagioclase inclusion (Fig. 5c). That is, the overall zoning in the garnet is unaffected by the presence of plagioclase inclusions, and garnet and plagioclase apparently have not interacted since the entrapment of the inclusions. The rims of the inclusions must, therefore, have been in equilibrium with the adjacent garnet at the conditions of garnet growth.

### THERMOBAROMETRY

The best estimate for the peak temperature experienced by sample HV104 comes from thermobarometry combining matrix phases with the garnet "well" [the low Fe/(Fe + Mg) region of the garnet just inside the rim; Spear 1991]. This estimate is in fact a minimum estimate of peak metamorphic temperature. The program TWEEQU (Berman 1991) gives estimates of 600–620 °C at 6000–6500 bars with various equilibria among the phases plagioclase + muscovite + biotite + garnet + kyanite ± staurolite ± rutile ± ilmenite, and different "well" analyses (see Lang 1990, 1991).

Some constraints can be placed on the changes in pressure and temperature during the growth of garnet by drawing thermobarometric curves for garnet + plagioclase equilibria with the use of compositions of adjacent garnet interior and plagioclase inclusions. Two thermobarometric equilibria that are particularly useful for this purpose are the garnet + plagioclase + aluminosilicate + quartz (GASP, Ghent 1976; Newton and Haselton 1981; Koziol and Newton 1988) and the garnet + muscovite + biotite + plagioclase (GMBP, Hodges and Spear 1982; Powell and Holland 1988; Hoisch 1990) equilibria.

Sample GMBP and GASP curves for garnet-interior-plagioclase-inclusion rim pairs (at the same radius) are shown in Figures 7a and 7b, respectively. Both equilibria have moderate slopes and are approximately parallel to the kyanite-sillimanite boundary. There are problems with applying either of these equilibria throughout the growth period of the garnet in sample HV104. The problem with applying the GASP equilibrium is that an aluminosilicate mineral was probably not present except during the growth of the rim of the garnet (see the discussion that follows). Ghent and Grover (1995), however, showed that the activity of  $Al_2SiO_5$  is commonly near 1.0 in staurolite-bearing metapelites that lack an aluminosilicate phase. All the phases required for the GMBP equilibrium were present throughout the growth of the garnet, but the composition of biotite almost certainly varied. Because biotite inclusions are rare in these garnets, and, if present, would have reequilibrated with surrounding garnet, a constant biotite composition equal to that of matrix biotite had to be used.

Despite their shortcomings, both equilibria show similar trends from the garnet core to the garnet rim. Garnet + plagioclase pairs nearest the core (curve 1) plot at the lowest temperature, highest pressure, or both. Pairs from the innermost part of the plagioclase inclusion-rich intermediate shell (curve 2) plot at nearly the highest temperature, lowest pressure, or both. Pairs from the outer part of the inclusion-rich intermediate shell (curve 3) plot at lower temperature, higher pressure, or both. Finally, the garnet "well" and matrix plagioclase (curve 4) yield the highest temperature, lowest pressure, or both. Although many  $P$ - $T$  paths might be compatible with these trends, the wide shaded lines in Figure 7 show simple paths that are consistent with the thermobarometry and what is known about the tectonics and deformation of the area. Formation of the nappe ( $F_{2a}$ , Fig. 1b) would have caused an abrupt thickening of the crust that would have produced high-pressure conditions, perhaps even below the temperature of the garnet isograd. An increase in temperature at nearly constant pressure would be expected to follow. Refolding of the nappe ( $F_{2b}$ ) would have caused additional thickening of the crust and a further increase in pressure. The temperature would be expected to continue to increase to peak metamorphic conditions.

#### GIBBS-METHOD $P$ - $T$ PATH

The  $P$ - $T$  path in Figure 8 was calculated using the Gibbs method (Spear 1990). Application of the Gibbs

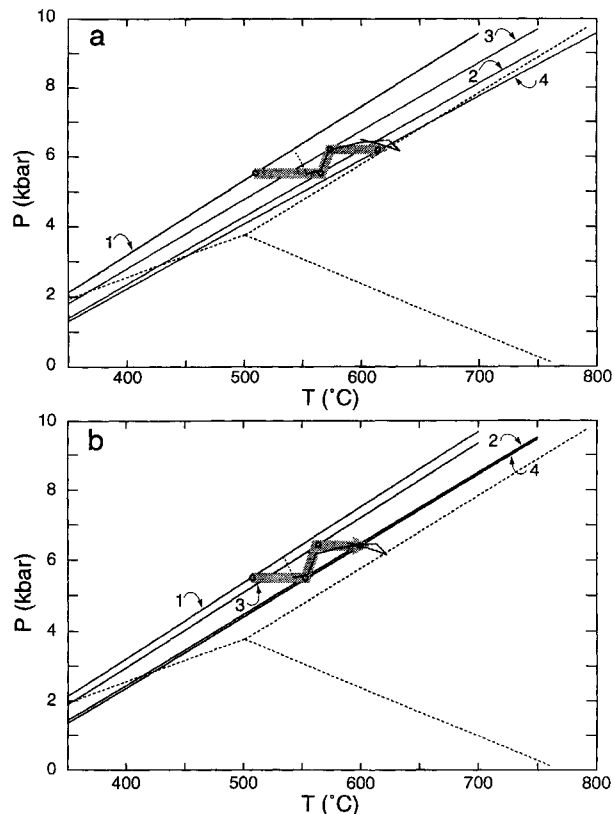
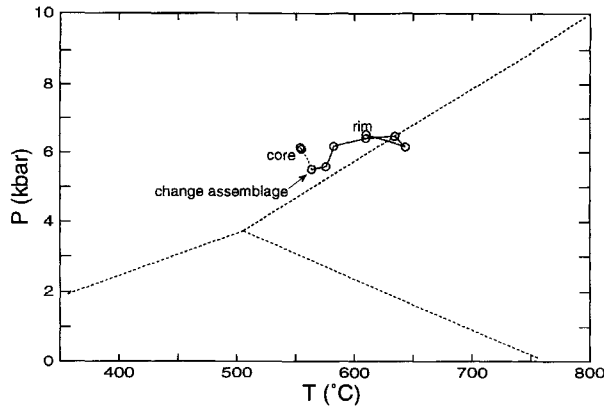


FIGURE 7. Thermobarometry for garnet + plagioclase-inclusion pairs from the HV104 garnet. (a) Isopleths for the garnet + muscovite + biotite + plagioclase (GMBP) geobarometer, using the calibration of Hodges and Crowley (1985) for four representative garnet + plagioclase pairs with matrix muscovite and biotite compositions. Plagioclase compositions are from analyses of plagioclase-inclusion rims, and garnet compositions are from the garnet profile at the appropriate radius. Isopleths are numbered sequentially from the core to the rim of the garnet. Representative garnet + plagioclase pairs come from the inner core (1,  $r = 0.4$  mm), the outer edge of the core (2,  $r = 1.3$  mm), the center of the intermediate plagioclase-inclusion-rich shell (3,  $r = 1.9$  mm), and the "well" near the garnet rim and matrix plagioclase (4,  $r > 3.1$  mm). The wide shaded line shows a possible  $P$ - $T$  path that is consistent with this geobarometer. Aluminosilicate phase boundaries and the Gibbs-method  $P$ - $T$  path from Figure 8 are shown for reference. (b) Isopleths for the garnet + aluminosilicate + silica + plagioclase (GASP) geobarometer, using the calibration of Koziol (1989) for the same four representative garnet-plagioclase pairs as in a with pure kyanite and quartz. The wide shaded line shows a possible  $P$ - $T$  path that is consistent with this geobarometer.

method requires knowledge of the mineral assemblage in which the garnet grew. The assemblage biotite + garnet + staurolite + muscovite + quartz + plagioclase is probably appropriate from about 1 mm away from the garnet center to the garnet rim, as is borne out by the DiffGibbs modeling discussed in the next section. The interior of the garnet, however, probably grew at the expense of



**FIGURE 8.** Gibbs-method  $P$ - $T$  path. This path was calculated assuming that the assemblage biotite + garnet + staurolite + muscovite + quartz + plagioclase was present from the garnet rim to within 1 mm of the center of the garnet. The assemblage was changed to chlorite + biotite + garnet + muscovite + quartz + plagioclase for the last two increments as indicated on the diagram. Connecting the two portions of the path is problematic because modeling indicated that garnet was consumed between the stages of growth in these two assemblages. The calculation began with the garnet rim at 610 °C, 6500 bars, the estimated peak conditions. Monitor parameters were spessartine, grossular, and almandine contents of garnet taken from the profile shown in Figure 4, and anorthite content of plagioclase-inclusion rims taken from Figure 6. An ideal solution model was used for garnet and all other phases. Measured compositions of matrix phases were used for starting compositions of phases other than garnet and plagioclase. Aluminosilicate phase boundaries are shown by dotted lines for reference.

chlorite in the assemblage chlorite + biotite + garnet + muscovite + quartz + plagioclase, as is typical of pelitic rocks of this composition (Spear 1993). The shoulder in garnet zoning at about 0.8–1.2 mm probably resulted largely from garnet consumption by the reaction chlorite + garnet = staurolite + biotite (Florence and Spear 1993; see below). Because kyanite was probably present only during growth of the outer rim of the garnet, it was not included in the mineral assemblage used to calculate the Gibbs path. The  $P$ - $T$  path in Figure 8 was calculated from the estimated peak metamorphic temperature in the assemblage biotite + garnet + staurolite + muscovite + quartz + plagioclase from the rim to 1.0 mm on the garnet profile. The final two steps of the Gibbs  $P$ - $T$  path (dotted portion on path in Fig. 8) were calculated with the assemblage chlorite + biotite + garnet + muscovite + quartz + plagioclase. The variance is such that the  $P$ - $T$  path can be determined from either assemblage if four monitor parameters are specified. Three independent garnet components at various positions along the profile in Figure 4 and the anorthite content of the rim of adjacent plagioclase inclusions provided the four required monitor parameters. Ideal solution behavior was assumed for garnet and all other minerals.

The Gibbs-method  $P$ - $T$  path shows a decrease in pres-

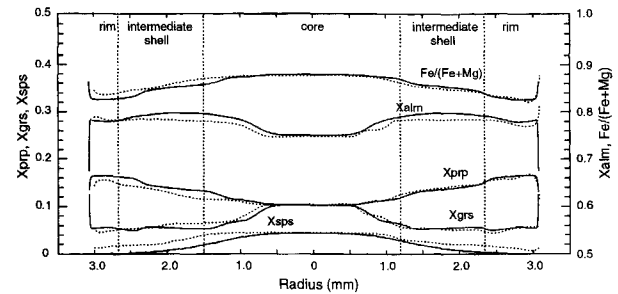


**FIGURE 9.** Garnet profiles for the most successful DiffGibbs model, shown with the measured profiles. The measured profiles from Figure 4 are shown as dotted lines, and the model profiles are shown as solid lines. Details of the correspondence of the measured and model profiles are discussed in the text.

sure during initial garnet growth in the chlorite + biotite + garnet assemblage. It further indicates garnet growth in the assemblage biotite + garnet + staurolite over a temperature range of 560–650 °C with an increase in pressure of approximately 700 bars between two constant pressure segments. The record of any path represented by garnet that was consumed to produce staurolite was lost. The outer two increments (garnet rim), which indicate a decrease in temperature, were probably strongly affected by diffusion and garnet consumption on cooling (Florence and Spear 1993; Spear 1990). The Gibbs-method  $P$ - $T$  path is consistent with thermobarometry, as is shown by the Gibbs path superimposed in Figure 7. The Gibbs path had to be shifted  $-10$  °C to be consistent with GMBP thermobarometry and  $-20$  °C to be consistent with GASP thermobarometry, but those shifts are within the uncertainties of the thermobarometers.

Several problems have been recognized with application of the Gibbs method for calculating  $P$ - $T$  paths (Frost and Tracy 1991). The necessity of knowing the assemblage in which the garnet grew has already been mentioned. In addition, there is strong evidence for consumption of a significant portion of the garnet to produce staurolite (see modeling below and Florence and Spear 1993). If garnet were consumed at any stage in the evolution of the rock, the record of that part of the  $P$ - $T$  path would be lost. Another problem with using the Gibbs method to calculate the  $P$ - $T$  path is that the outer part of the garnet profile almost certainly results from diffusion (Spear 1991) rather than garnet growth. Forward modeling, that is, modeling of garnet growth from its inception, can be performed using the computer program DiffGibbs (Florence and Spear 1993; Spear and Florence 1992; Spear 1989, 1990). It incorporates diffusion and allows one to examine the effects of various changes in mineral assemblage and  $P$ - $T$  path. DiffGibbs, therefore, overcomes some of the problems that have been noted with Gibbs-method calculations. DiffGibbs modeling is a trial-and-error process, the goal of which is to match the observed zoning in garnet within the constraints provided by other geologic evidence.

TABLE 2. Input data: Mode and mineral compositions at the garnet isograd

	Point count (vol%)	Calc. vol% (at garnet isograd)	Modified vol%	$X_{Mg}$	$X_{Fe}$	$X_{Mn}$	$X_{Ca}$	$X_{Na}$
Quartz	27	28	44					
Muscovite	26	30	36					0.170
Garnet	14	0	0	0.104	0.749	0.045	0.103	
Biotite	14	7	7	0.464	0.534	0.002		
Plagioclase	14	14	3				0.330	0.670
Chlorite		21	10	0.488	0.511	0.001		
Staurolite	1							
Kyanite	4							
H <sub>2</sub> O		0	0					

## DIFFGIBBS MODELING

### Method

The program DiffGibbs combines the Gibbs technique for calculating mineral growth and consumption along a prescribed  $P$ - $T$  path with a diffusion module for calculating the effects of intracrystalline diffusion in garnet (Spear 1988, 1990; Florence and Spear 1991, 1993; Spear and Florence 1992). The first step in the procedure is the Gibbs step. In this step, the program monitors the amounts and compositions of all phases in the rock and generates a zoning profile for fractionally crystallized garnet over a specified increment of temperature and pressure. Mass balance is maintained, and garnet and H<sub>2</sub>O are fractionated. In the second step, the diffusion step, the program uses a finite-difference algorithm to calculate the effect of intracrystalline diffusion in the garnet on the zoning profile over the elapsed time interval.

Use of the program involves specifying an initial assemblage and incrementally applying a Gibbs step followed by a diffusion step over a particular  $P$ - $T$  path. Model garnet growth begins at conditions estimated for the garnet isograd, and minerals are added to or removed from the reacting assemblage at appropriate conditions. Heating and cooling rates must be specified over the entire path. Ideal solution models were used for all phases. Because of the many uncertainties in the input parameters, the added precision of nonideal solution models was not thought to be justified. Models were tested and refined by comparing calculated garnet profiles and plagioclase compositions to the measured garnet profiles and plagioclase-inclusion compositions in HV104.

### Diffusion coefficients

Tracer diffusion coefficients for the various components in garnet were determined by Loomis et al. (1985) and by Chakraborty and Ganguly (1992). The diffusion coefficients of Loomis et al. (1985) were used for most HV104 model experiments, including the model shown in Figure 9, because they maximize the effects of diffusion and result in a slightly better fit to the shape of the outer garnet-rim profile. These diffusion coefficients are approximately 1.5 orders of magnitude larger than those of Chakraborty and Ganguly (1992), resulting in faster diffusion of garnet components. Similar results may be

obtained by using the slower diffusion coefficients of Chakraborty and Ganguly (1992) in combination with slower cooling rates (see Spear and Florence 1992; Spear et al. 1995).

### Initial assemblage

The assemblage from which the garnet grew, beginning at the garnet isograd, is presumed to have been chlorite + biotite + muscovite + quartz + plagioclase (Table 2). This assemblage is typical of normal low-grade pelitic rocks, and there is no evidence that this rock contained any other minerals in the NCKFMASH system below the garnet isograd. Accessory minerals such as graphite, ilmenite, sulfides, and tourmaline do not affect phase relations among NCKFMASH minerals and were omitted from the modeling. The initial garnet composition was considered to be that of the core of the analyzed garnet. Compositions of other minerals in equilibrium with that garnet at the starting temperature and pressure were calculated from calibrated exchange equilibria (Table 2). Uncertainty exists concerning the relative partitioning of Mn between chlorite and biotite; however, analyses of chlorite and biotite in equilibrium with the rim of an unusually spessartine-rich garnet from another area (Lang, unpublished analyses) indicate conclusively that biotite accommodates more Mn than coexisting chlorite.

The initial mode at the garnet isograd was calculated from the mode determined by a point count of the HV104 polished section (Table 2). To calculate the initial mode, the Gibbs method (with mass balance) was run from the peak temperature to low temperature at constant pressure, allowing consumption of higher grade phases in favor of lower grade phases until all kyanite, staurolite, and garnet were used up. This is essentially the reverse of DiffGibbs modeling. Although this method is overly simple, it gives an approximation of the initial amounts of phases. Results of the point count and calculated initial modes and mineral compositions are given in Table 2.

To match successfully the amounts and compositions of minerals with DiffGibbs modeling, it was necessary to modify the initial mode. To match the observed decrease in anorthite content of the plagioclase during garnet growth, it was necessary to decrease the initial amount of plagioclase. The initial amount of chlorite was de-

**TABLE 3.** DiffGibbs model parameters

Thermodynamic data	Berman 1988, modified 1990 (personal communication)
Diffusion coefficients	Loomis et al. 1985
Nucleation density	15 per 100 cm <sup>3</sup>
Starting <i>P</i> , <i>T</i>	550 °C at 6500 bars
Heating rate	25 °C/Ma
Cooling rate	25 °C/Ma

creased, so that chlorite was consumed to form staurolite at the appropriate stage of garnet consumption. Decreases in amounts of chlorite and plagioclase were compensated by an increase in initial quartz. The calculated initial mode is approximate, and adjustments in it may be justified by the likelihood of open-system behavior during metamorphism. Some quartz was undoubtedly lost from the rock, and Na infiltration may have increased the final amount of plagioclase. The amount of plagioclase (some of which is not twinned) may have been overestimated in the point count. The modified initial mode is also shown in Table 2. A nucleation density of 15 garnet grains per 100 cm<sup>3</sup> was used because it produced model garnet with the same radius as the analyzed garnet and similar compositional profiles.

#### The model

Moderately successful DiffGibbs models were achieved by using a simple *P-T* path with an isobaric segment at 5500 bars from approximately 550 to 580 °C, a pressure increase segment from 580 °C at 5500 bars to 590 °C at 6000 bars, and an additional isobaric segment to approximately 615 °C. Changes in mineral assemblage were made at temperatures inferred from the petrogenetic grid of Spear and Cheney (1989). This *P-T* path is a simplification of the Gibbs-method path (Fig. 8) and is consistent with the thermobarometry (Fig. 7). A much better match of the model profiles with the measured profiles, especially in the vicinity of the two-step shoulder in mole-fraction grossular on the right side of Figure 4, resulted when mole-fraction grossular and mole-fraction spessartine were used as monitor parameters (instead of pressure and temperature) for that part of the model.

Profiles of garnet components from the most successful model are shown with the measured profiles in Figure 9. The right side of the grossular profile was matched as closely as possible, so the success of the match for other components is a test of the model. Model parameters are given in Table 3, and the *P-T* path that produced the successful model profiles is shown in Figure 10. This *P-T* path is very similar to the path calculated by the Gibbs method (Fig. 8) and is consistent with thermobarometry (Fig. 7). Although the actual path is not tightly constrained, a path of this shape is required for successful modeling. The nearly isobaric heating path is similar to those calculated by Thompson and England (1984) following crustal thickening. The early pressure decrease in the path may indicate decompression from an early episode of crustal thickening at low temperature. The later

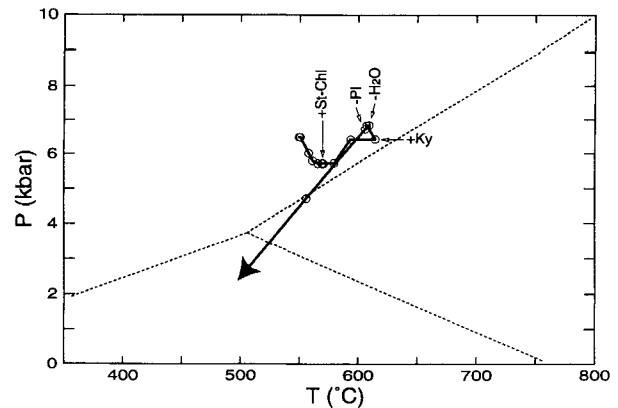


**FIGURE 10.** *P-T* path for the most successful model. The path starts at 550 °C at 6500 bars and reaches its maximum temperature at 614 °C at 6474 bars, near the kyanite-sillimanite boundary (dotted lines show aluminosilicate phase boundaries for reference). Conditions at which phases were added to or removed from the assemblage are shown.

pressure increase seems to indicate thickening during metamorphic heating, perhaps corresponding to  $F_{2b}$  deformation. In the absence of precise geochronologic constraints, a heating rate of 25 °C/Ma was used in all simulations (Florence and Spear 1993). Results of the modeling are not particularly sensitive to the heating rate.

In the most successful model, garnet growth began at 550 °C and 6500 bars in the assemblage chlorite + biotite + garnet + muscovite + plagioclase + quartz. These initial conditions are consistent with Gibbs-method modeling and thermobarometry. A nucleus of garnet ( $r = 757 \mu\text{m}$ ) was allowed to grow over a 1 °C temperature increment at constant pressure. The next three increments of garnet growth were constrained by changes in mole-fraction grossular and spessartine from the measured profile so that the details of garnet zoning could be matched. With these increments, garnet grew to 1445  $\mu\text{m}$  with decreasing pressure and increasing temperature to 566 °C at 5724 bars. Grossular decreased abruptly as a direct consequence of the pressure decrease, an increase in almandine compensated for the decrease in grossular, but pyrope and spessartine were hardly affected. At this point temperature and pressure were again chosen as monitor parameters. Garnet growth was allowed to proceed to 570 °C at constant pressure in this low-grade assemblage until the garnet radius was approximately 1.9 mm. Staurolite (in exchange equilibrium with the garnet) was introduced at 570 °C on the basis of the petrogenetic grid of Spear and Cheney (1989). Florence and Spear (1993) demonstrated convincingly that garnet was consumed to produce staurolite in metapelites from the Littleton Formation in New Hampshire and suggested that garnet consumption that produces staurolite is common in normal pelites (see also Spear et al. 1990; Spear 1991). The outer step in grossular (right side of the grossular profile in Fig. 3) and the shoulders in the profiles of spessartine and pyrope are

inferred to have resulted from partial garnet consumption. Garnet consumption and production of staurolite were, therefore, allowed to proceed to the edge of the core region and the shoulders of the profiles of all garnet components at approximately 1.3 mm radius (Fig. 4). It was necessary to reduce the estimated amount of chlorite in the initial assemblage to avoid consuming all the garnet before chlorite was used up. Staurolite growth at the expense of garnet and chlorite occurred in the model over the narrow temperature range of 0.7 °C at constant pressure. At this stage (570.6 °C at 5724 bars), chlorite was removed from the assemblage.

Considerable garnet growth (approximately 60% of the garnet radius, or approximately 92% of the garnet volume) must have occurred after this stage of garnet consumption to produce the plagioclase inclusion-rich shell and the inclusion-free rim of the garnet. There are rare small inclusions of staurolite in the inclusion-rich intermediate shell of garnet in HV104 and other kyanite-bearing samples, but no kyanite inclusions were observed, except in the outermost garnet rims and extending into the matrix. On the basis of these relationships, it is probable that the inclusion-rich intermediate shell of garnet grew in the presence of staurolite in the assemblage biotite + garnet + staurolite + muscovite + quartz + plagioclase and that the outer inclusion-free rim of garnet grew in the presence of kyanite (and staurolite, which was never completely consumed).

In a similar situation Florence and Spear (1993, case 2) did not infer substantial growth of garnet in the assemblage biotite + garnet + staurolite. Contours of moles of garnet in  $P$ - $T$  space for the assemblage biotite + garnet + staurolite (Fig. 11; Spear 1988, 1989) suggest that a difference in  $P$ - $T$  path might explain the difference in garnet growth between this occurrence and that studied by Florence and Spear (1993). In the kyanite field in the vicinity of 6 kbar, contours of moles of garnet are nearly isobaric (Fig. 11). Consequently, along a path of gradually increasing pressure with increasing temperature, such as that used by Florence and Spear (1993), garnet growth is limited (Fig. 11). If, however, the  $P$ - $T$  path shows a significant pressure increase at nearly constant temperature, garnet growth in the assemblage biotite + garnet + staurolite would be expected to be substantial (Fig. 11). For the study area, a path with a significant pressure increase at an intermediate stage of metamorphism is indicated by the structural interpretation, thermobarometry, and Gibbs method. A path with a steep increase in pressure in the assemblage biotite + garnet + staurolite is required to produce significant garnet growth in the model for HV104.

In the most successful model, temperature was allowed to continue to increase after removal of chlorite at constant pressure to 580 °C. Garnet growth from a radius of approximately 1.3–2.4 mm was produced by a pressure increase at 50 bars/°C from 5724 bars at 580 °C to 6474 bars at 595 °C. This portion of the path produced the intermediate plateaus in the grossular and pyrope profiles.

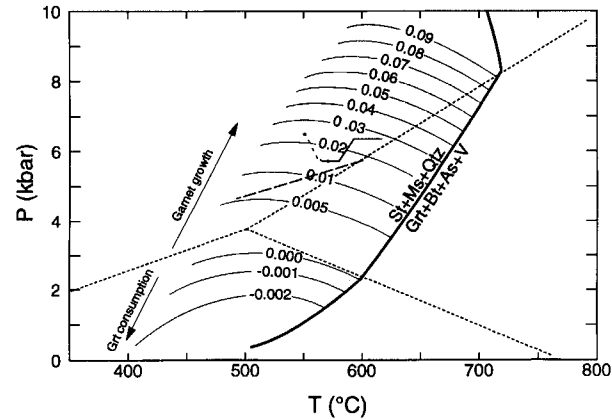
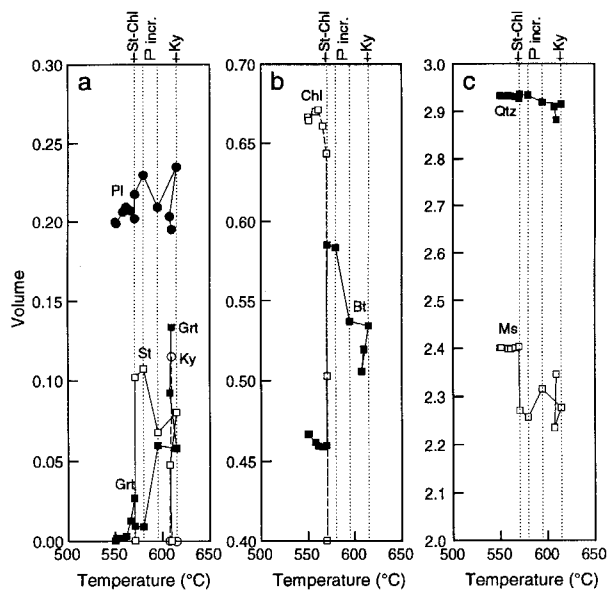


FIGURE 11. Contours of moles of garnet in the assemblage biotite + garnet + staurolite + muscovite + quartz in  $P$ - $T$  space calculated using the Gibbs method. The location of the reaction  $St + Ms + Qtz = Grt + Bt + As + V$ , which is the upper limit of this assemblage, is taken from the petrogenetic grid of Spear and Cheney (1989). A portion of the  $P$ - $T$  path for the successful model of this study is shown as a dotted (assemblage  $Chl + Bt + Grt + Ms + Qtz$ ), then solid (assemblage  $Bt + Grt + St + Ms + Qtz$ ) line. A representative path from the study of Florence and Spear (1993) is shown as a dashed line. Aluminosilicate phase boundaries are shown as dotted lines for reference.

The decrease in grossular at 2.4 mm, which is accompanied by a slight increase in pyrope and a slight decrease in spessartine, suggests another episode of slow growth or consumption of garnet. The decrease in grossular can be matched by minimal garnet growth with increasing temperature (595–615 °C) at constant pressure (6474 bars).

The inclusion-free outer rim of the garnet (beginning at the “well” in grossular content) grew in the presence of kyanite, along with staurolite, which was never completely consumed. In the model, kyanite was added to the assemblage at 615 °C. The “well” in grossular content, which is apparent on the measured profile (Figs. 4 and 9) and in many of the compositional images of garnet from staurolite + kyanite samples from the Maryland Piedmont (Fig. 3a), suggests that increasing pressure resulted in the increase in grossular. It was not possible to reproduce the increase beyond the grossular “well” by any path with increasing temperature and increasing pressure. A very good match to the well and the outer part of the profile was, however, achieved when  $X_{\text{grossular}}$  and  $X_{\text{spessartine}}$  were used as monitor parameters (instead of pressure and temperature) for one increment. Use of these monitors resulted in an increase in pressure with decreasing temperature to 607 °C at 6841 bars. The remainder of the outer garnet rim (right side of profile) was successfully modeled by garnet growth in the presence of kyanite and staurolite with a 2 °C increase in temperature at constant pressure. Plagioclase consumption during this stage of garnet growth (Fig. 12) is consistent with the inclusion-free nature of the garnet rim. Peak temperature conditions



**FIGURE 12.** Calculated modes from the most successful model for all mineral phases included in the model as a function of temperature. The temperature at which staurolite was added and chlorite removed, the temperature range of the pressure increase, and the temperature at which kyanite was added are indicated by vertical dotted lines. (a) Abundances of garnet, staurolite, kyanite, and plagioclase; (b) abundances of biotite and chlorite; (c) abundances of muscovite and quartz.

of 615 °C at 6474 bars in the model (which correspond to the “well” in grossular) are within the limits of thermobarometric estimates. However, the effects of diffusion are likely to cause an underestimate of peak metamorphic temperature (Spear 1991). In fact, the maximum temperature calculated from the model-garnet profile (after cooling to 500 °C) with matrix biotite was 20 °C lower than the maximum model temperature.

Cooling of the assemblage from 609 °C and 6841 bars is problematic because the actual cooling path is not well known. Although the actual cooling path is unlikely to have had a constant slope (Thompson and England 1984), a cooling path with a slope of 40 bars/°C was used as a first approximation. The actual cooling path is known to have entered the sillimanite field because this sample and many others from the area contain small amounts of fine, late sillimanite (Lang 1990). Removal of H<sub>2</sub>O from the assemblage as cooling began prevented dehydration equilibria from proceeding. Removal of H<sub>2</sub>O was justified because all but a small amount of pore fluid would have escaped from the rock at the peak temperature. Because the assemblage includes garnet, muscovite, biotite, plagioclase, quartz, and aluminosilicate, both of the equilibria upon which the GASP and GMBP geobarometers are based would be active, even in the absence of H<sub>2</sub>O. These reactions consume garnet along *P-T* paths steeper than the thermobarometric isopleths (approximately 20 bars/°C,

Fig. 7). At high temperatures, these equilibria are probably active and consume some garnet on the retrograde path. Because they involve plagioclase, which is refractory, they are likely to be ineffective below some limiting temperature. In this particular model, plagioclase was removed from the assemblage after cooling to 606 °C (at a garnet radius of 3100 μm) to arrest these reactions and allow only Fe-Mg-Mn exchange reactions to continue. A constant cooling rate of 25 °C/m.y. was used for the model shown in Figure 9. This represents a high rate for erosional exhumation, but it has recently been suggested (Spear et al. 1995; Spear 1995) that initial cooling rates for regional metamorphic rocks that experience tectonic denudation may be much more rapid (hundreds to thousands of degrees per Ma). Cooling was allowed to proceed to 500 °C.

## DISCUSSION

The right halves of the measured pyrope, grossular, and Fe/(Fe + Mg) profiles are matched quite well by the model, as shown in Figure 9. Almandine, spessartine, and the left halves of the profiles of other components are matched slightly less well. The general shapes of the model profiles are remarkably similar to those of the measured profiles. Only slight modifications of the model parameters would be required to match the left halves of the profiles (rather than the right halves), and garnet would not be expected to grow in a perfect radially symmetric fashion. The modeling indicates that the shoulder of the irregular grossular-rich, almandine-poor inner core resulted from an early decrease in pressure and that the outer step in the grossular profile and the shoulders in the pyrope and spessartine profiles at greater radius resulted from garnet consumption to produce staurolite. Reversals for all components except almandine at the garnet rim are matched fairly well by the model. Although measured almandine increases at the rim (right side of profile), in the model, almandine decreases dramatically at the rim except for a very slight increase. Garnet consumption on cooling by continuous reactions among garnet, muscovite, biotite, plagioclase, and aluminosilicate causes an increase in almandine, but this trend is reversed when plagioclase is removed so that only the exchange reactions can continue. Because there is very little biotite in the immediate vicinity of the garnet, Fe-Mg exchange may have been ineffective in producing the decrease in almandine predicted by the model.

The compositions of the plagioclase inclusions provide an additional constraint on the model. The anorthite content of plagioclase inclusions in the HV104 garnet is shown in Figure 6 as a function of distance from the center of the HV104 garnet. The composition of model plagioclase is superimposed on the graph of plagioclase composition as a function of garnet radius in Figure 6. The amount of plagioclase grown in the model is shown in Figure 12, along with modal changes in other minerals as a function of temperature. Model anorthite content matches the compositions of plagioclase-inclusion rims

very well (Fig. 6). The cores of plagioclase inclusions in the inclusion-rich intermediate shell of the garnet may be relicts of earlier plagioclase, but their rims apparently grew as garnet was being consumed to produce staurolite. Note the increase in the volume of plagioclase, which corresponds to a decrease in the volume of garnet in the vicinity of 570 °C (Fig. 12).

The intermediate shell of the garnet ( $r = 1.3\text{--}2.3$  mm) is inferred to have grown from 580 to 593 °C with increasing pressure in the assemblage biotite + garnet + staurolite. According to the model, while garnet grew, the amount of plagioclase decreased slightly and its anorthite content remained approximately constant (Figs. 6 and 12). Model anorthite composition matches measured plagioclase-rim compositions very well. Again according to the model, garnet growth nearly ceased (the radius decreased from 2.42 to 2.40 mm) as temperature increased from 595 to 615 °C, while plagioclase with decreasing anorthite content grew. The model predicts that plagioclase would be consumed and equilibrium anorthite content would remain at about 24 mol% after the introduction of kyanite. The fact that the garnet rim, which is believed to have grown in the presence of kyanite, contains very few inclusions of plagioclase or any other phase is therefore consistent with the model. Rims of matrix plagioclase grains have an anorthite content of approximately 23 mol%, consistent with the model.

The results of this modeling contrast in several important ways with those of the modeling by Florence and Spear (1993) for rocks of similar bulk composition and metamorphic grade. Significant differences result from the fact that the garnet in HV104 experienced considerable growth in the assemblage biotite + garnet + staurolite after the episode of garnet (+ chlorite) consumption to produce staurolite (+ biotite). The garnet modeled here, therefore, has a complex interior profile that was produced by two significant stages of growth. This garnet is also larger than those modeled by Florence and Spear (1993) and Spear et al. (1995). Its interior was therefore much less affected by diffusion. Florence and Spear (1993) found that thermobarometry that involves garnet from staurolite- and kyanite-grade rocks yielded serious underestimates of peak metamorphic temperatures. Aside from the small underestimate of peak temperature resulting from the effects of diffusion on cooling, the thermobarometric estimate of 600–620 °C is believed to be accurate because considerable garnet growth occurred after the major episode of garnet consumption.

The faster diffusion coefficients of Loomis et al. (1985) were used in the model shown in Figure 9. If the diffusion coefficients of Chakraborty and Ganguly (1992) were used instead, spessartine in the core would be very slightly higher, and the upturn or downturn in various components at the rim would be significantly sharper. Because the upturn or downturn in the model profiles is already more abrupt than the measured profiles, the diffusion coefficients of Loomis et al. (1985) seem to be slightly preferable. A faster cooling rate would affect the outer part

of the profile in a way similar to that caused by the slower diffusion coefficients.

## CONCLUSIONS

Garnet grains from any given hand sample in the study area tend to be similar in size and have similar zoning and inclusion patterns. Although garnet similar to the modeled garnet from HV104 is common in the study area, garnet from some samples is rich in plagioclase inclusions but lacks the irregular core with high grossular and low almandine contents, and garnet from other samples is small, relatively homogeneous, inclusion-free, and postkinematic (Hall 1988). Garnet that lacks the irregular grossular-rich core may have resulted from almost complete consumption of garnet (+ chlorite) to form staurolite, and diffusion may have destroyed, or the thin section may have missed, the small relict of the early core. In rocks that contain the small postkinematic garnet, early garnet may have been completely consumed to form staurolite. The small, late, inclusion-free garnet grains would then represent a second generation of garnet that grew in the assemblage biotite + garnet + staurolite with increasing pressure. Even in samples like HV104, early formed garnet was probably quite variable in size (Cashman and Ferry 1988). Smaller garnet grains would have been consumed first by the reaction garnet + chlorite = staurolite + biotite, leaving only the cores of larger garnet grains to act as nuclei for continued garnet growth. Nucleation density (the number of grains per 100 cm<sup>3</sup>), therefore, changed during the reaction history of individual samples. Early consumption of small garnet grains may help to explain the relative uniformity in the size of grains from individual hand specimens from the study area.

This type of modeling confirms that metamorphism is a dynamic process that involves growth and consumption of even the most refractory and porphyroblastic phases (garnet and plagioclase) along relatively simple  $P$ - $T$  paths (see also Florence and Spear 1993). To the extent that the modeling and input parameters such as heating and cooling rates and diffusion coefficients are accurate, episodes of garnet consumption may not leave distinctive spikes or steps in the compositional profiles of garnet.

## ACKNOWLEDGMENTS

Frank Spear provided the computer programs for the Gibbs method and diffusion calculations. I thank him for helping me learn to use the programs to gain a better understanding of metamorphic rocks, for engaging in lengthy discussions of the modeling presented here, and for providing a thorough review of the manuscript. I thank Donna Whitney for providing additional microprobe analyses and for a very helpful review of the manuscript. I thank Frank Spear, Synnøve Elvevold, Nathalie Marchildon, Bill Minarik, and Jane Gilotti for many stimulating discussions about garnet growth and zoning during my sabbatical at Rensselaer Polytechnic Institute. Frank Florence provided many specific and helpful suggestions concerning the use of DiffGibbs to interpret staurolite + kyanite-bearing pelitic rocks. I thank Dave Wark for assistance with the microprobe at R.P.I. and Todd Solberg for assistance with the microprobe at Virginia Polytechnic Institute and State University. Pam Hall is thanked for helping to collect the samples and for interpreting the textures. This research was supported in part by National Science Foundation grant EAR-871034.

## REFERENCES CITED

- Albee, A.L., and Ray, L. (1970) Correction factors for electron probe microanalysis of silicates, oxides, carbonates, phosphates and sulfates. *Analytical Chemistry*, 42, 1408–1414.
- Bence, A.E., and Albee, A.L. (1968) Empirical correction factors for the electron microanalysis of silicates and oxides. *Journal of Geology*, 76, 382–403.
- Berman, R.G. (1988) Internally-consistent thermodynamic data for minerals in the system  $\text{Na}_2\text{O}-\text{K}_2\text{O}-\text{CaO}-\text{MgO}-\text{FeO}-\text{Fe}_2\text{O}_3-\text{Al}_2\text{O}_3-\text{SiO}_2-\text{TiO}_2-\text{H}_2\text{O}-\text{CO}_2$ . *Journal of Petrology*, 29, 445–522.
- (1991) Thermobarometry using multi-equilibrium calculations: A new technique, with petrological applications. *Canadian Mineralogist*, 29, 833–855.
- Brown, M. (1993) *P-T-t* evolution of orogenic belts and the causes of regional metamorphism. *Journal of the Geological Society, London*, 150, 227–241.
- Cashman, K.V., and Ferry, J.M. (1988) Crystal size distribution (CSD) in rocks and the kinetics and dynamics of crystallization. *Contributions to Mineralogy and Petrology*, 99, 401–415.
- Chakraborty, S., and Ganguly, J. (1992) Cation diffusion in aluminosilicate garnets: Experimental determination in spessartine-almandine diffusion couples, evaluation of effective binary diffusion coefficients, and applications. *Contributions to Mineralogy and Petrology*, 111, 74–86.
- Crowley, W.P., Reinhardt, J., and Cleaves, E.T. (1976) Geologic map of Baltimore County and City. Maryland Geological Survey.
- England, P.C., and Thompson, A.B. (1984) Pressure-temperature-time paths of regional metamorphism: Part I. Heat transfer during the evolution of regions of thickened continental crust. *Journal of Petrology*, 25, 894–928.
- Fisher, G.W. (1989) Petrology and structure of gneiss anticlines near Baltimore, Maryland. 28th International Geological Congress Field Trip Guidebook T204, American Geophysical Union, 12 p.
- Fisher, G.W., Higgins, M.W., and Zietz, I. (1979) Geological interpretations of aeromagnetic maps of the crystalline rocks in the Appalachians, northern Virginia to New Jersey. Maryland Geological Survey Report of Investigations, 32.
- Florence, F.P., and Spear, F.S. (1991) Effects of diffusional modification of garnet growth zoning on *P-T* path calculations. *Contributions to Mineralogy and Petrology*, 107, 487–500.
- (1993) Influences of reaction history and chemical diffusion on *P-T* calculations for staurolite schists from the Littleton Formation, northwestern New Hampshire. *American Mineralogist*, 78, 345–359.
- Frost, B.R., and Tracy, R.J. (1991) *P-T* paths from zoned garnets: Some minimum criteria. *American Journal of Science*, 291, 917–939.
- Ghent, E.D. (1976) Plagioclase-garnet- $\text{Al}_2\text{SiO}_5$  quartz: A potential geobarometer-geothermometer. *American Mineralogist*, 61, 710–714.
- Ghent, E.D., and Grover, T.W. (1995) Calculation of the activity of  $\text{Al}_2\text{SiO}_5$ : Applications to the geobarometry and geothermometry of garnet and staurolite zone metapelitic rocks. *American Journal of Science*, 295, 923–942.
- Hall, P.S. (1988) Deformation and metamorphism of the aluminous schist member of the Setters Formation, Cockeysville, Maryland, 99 p. M.S. thesis, West Virginia University, Morgantown.
- Hodges, K.V., and Spear, F.S. (1982) Geothermometry, geobarometry and the  $\text{Al}_2\text{SiO}_5$  triple point at Mt. Moosilauke, New Hampshire. *American Mineralogist*, 67, 1118–1134.
- Hodges, K.V., and Crowley, P.D. (1985) Error estimation and empirical geothermobarometry for pelitic systems. *American Mineralogist*, 70, 702–709.
- Hoisch, T.D. (1990) Empirical calibration of six geobarometers for the mineral assemblage quartz + muscovite + biotite + plagioclase + garnet. *Contributions to Mineralogy and Petrology*, 104, 225–234.
- Kohn, M.J., Orange, D.L., Spear, F.S., Rumble, D., III, and Harrison, T.M. (1992) Pressure, temperature, and structural evolution of west-central New Hampshire: Hot thrusts over cold basement. *Journal of Petrology*, 33, 521–556.
- Koziol, A.M. (1989) Recalibration of the garnet-plagioclase- $\text{Al}_2\text{SiO}_5$ -quartz (GASP) geobarometer and application to natural parageneses. *Eos*, 70, 493.
- Koziol, A.M., and Newton, R.C. (1988) Redetermination of the anorthite breakdown reaction and improvement of the plagioclase-garnet- $\text{Al}_2\text{SiO}_5$ -quartz geobarometer. *American Mineralogist*, 73, 216–223.
- Lang, H.M. (1990) Regional variation in metamorphic conditions recorded by pelitic schists in the Baltimore area, Maryland. *Southeastern Geology*, 31, 27–43.
- (1991) Quantitative interpretation of within-outcrop variation in metamorphic assemblage in staurolite-kyanite-grade metapelites, Baltimore, Maryland. *Canadian Mineralogist*, 29, 655–671.
- Loomis, T.P., Ganguly, J., and Elphick, S.C. (1985) Experimental determinations of cation diffusivities in aluminosilicate garnets: II. Multi-component simulation and tracer diffusion coefficients. *Contributions to Mineralogy and Petrology*, 90, 45–51.
- Muller, P.D., and Chapin, D.A. (1984) Tectonic evolution of the Baltimore Gneiss anticlines, Maryland. Geological Society America Special Paper, 194, 127–148.
- Muller, P.D., Candela, P.A., and Wylie, A.G. (1989) Liberty Complex: Polygenetic melange in the central Maryland Piedmont. Geological Society of America Special Paper, 228, 113–133.
- Newton, R.C., and Haselton, H.T. (1981) Thermodynamics of the garnet-plagioclase- $\text{Al}_2\text{SiO}_5$ -quartz geobarometer. In R.C. Newton, A. Navrotsky, and B.J. Wood, Eds., *Thermodynamics of minerals and melts*, p. 131–147. Springer-Verlag, New York.
- Powell, R., and Holland, T.J.B. (1988) An internally consistent thermodynamic dataset with uncertainties and correlations: 3. Applications to geobarometry, worked examples and a computer program. *Journal of Metamorphic Geology*, 6, 173–204.
- Sinha, A.K. (1988) Granites and gabbros: A field excursion through the Maryland Piedmont, 19 p. V.M. Goldschmidt Conference, Baltimore, Maryland.
- Solberg, T.N., and Speer, J.A. (1982) QALL, A 16-element analytical scheme for efficient petrologic work on an automated ARL-SEM: Application to mica reference samples. In K.F.J. Heinrich, Ed., *Microbeam analysis*, San Francisco, California.
- Spear, F.S. (1988) The Gibbs method and Duhem's theorem: The quantitative relationships among *P*, *T*, chemical potential, phase composition and reaction progress in igneous and metamorphic systems. *Contributions to Mineralogy and Petrology*, 99, 249–256.
- (1989) Petrologic determination of metamorphic pressure-temperature-time paths. In American Geophysical Union Short Course in Geology, 7, 1–55.
- (1990) Computer exercises for *P-T* path calculations, Macintosh version. In F.S. Spear and S.M. Peacock, Eds., *Metamorphic P-T-t paths: Program manual and computer exercises for the calculation of metamorphic phase equilibria, pressure-temperature-time paths and thermal evolution of orogenic belts*, p. 1–126.
- (1991) On the interpretation of peak metamorphic temperatures in light of garnet diffusion during cooling. *Journal of Metamorphic Geology*, 9, 379–388.
- (1993) Metamorphic phase equilibria and pressure-temperature-time paths. *Mineralogical Society of America Monograph*, 799 p.
- (1995) How fast can regional metamorphic rocks cool? *Eos*, 76, S290.
- Spear, F.S., and Selverstone, J. (1983) Quantitative *P-T* paths from zoned minerals: Theory and tectonic applications. *Contributions to Mineralogy and Petrology*, 83, 348–357.
- Spear, F.S., Selverstone, J., Hickmott, D., Crowley, P., and Hodges, K.V. (1984) *P-T* paths from garnet zoning: A new technique for deciphering tectonic processes in crystalline terranes. *Geology*, 12, 87–90.
- Spear, F.S., and Cheney, J.T. (1989) A petrogenetic grid for pelitic schists in the system  $\text{SiO}_2-\text{Al}_2\text{O}_3-\text{FeO}-\text{MgO}-\text{K}_2\text{O}-\text{H}_2\text{O}$ . *Contributions to Mineralogy and Petrology*, 100, 149–164.
- Spear, F.S., Kohn, M.J., Florence, F.P., and Menard, T. (1990) A model for garnet and plagioclase growth in pelitic schists: Implications for thermobarometry and *P-T* path determinations. *Journal of Metamorphic Geology*, 8, 683–696.
- Spear, F.S., and Florence, F.P. (1992) Thermobarometry in granulites: Pitfalls and new approaches. *Journal of Precambrian Research*, 55, 209–241.
- Spear, F.S., Kohn, M.J., and Paetzold, S. (1995) Petrology of the regional sillimanite zone, west-central New Hampshire, U.S.A., with implica-

- tions for the development of inverted isograds. *American Mineralogist*, 80, 361–376.
- St-Onge, M.R. (1987) Zoned poikiloblastic garnets: *P-T* paths and syn-metamorphic uplift through 30 km of structural depth, Wopmay Orogen, Canada. *Journal of Petrology*, 28, 1–21.
- Thompson, A.B., Tracy, R.J., Lyttle, P., and Thompson, J.B. (1977) Prograde reaction histories deduced from compositional zonation and mineral inclusions in garnet from the Gassetts schist, Vermont. *American Journal of Science*, 277, 1152–1167.
- Thompson, A.B., and England, P.C. (1984) Pressure-temperature-time paths of regional metamorphism: II. Their influence and interpretation using mineral assemblages in metamorphic rocks. *Journal of Petrology*, 25, 929–955.
- Tracy, R.J., Robinson, P., and Thompson, A.B. (1976) Garnet composition and zoning in the determination of temperature and pressure of metamorphism, central Massachusetts. *American Mineralogist*, 61, 762–775.
- Whitney, D.L. (1991) Calcium depletion halos and Fe-Mn-Mg zoning around faceted plagioclase inclusions in garnet from a high-grade pelitic gneiss. *American Mineralogist*, 76, 493–500.

MANUSCRIPT RECEIVED JULY 24, 1995

MANUSCRIPT ACCEPTED JULY 19, 1996